TWENTY FIRST EUROPEAN ROTORCRAFT FORUM

Paper No. VII-8

THE EFFECT OF INFLOW MODELS ON THE DYNAMIC RESPONSE OF HELICOPTERS

U.T.P. Arnold, J.D. Keller, H.C. Curtiss

PRINCETON UNIVERSITY
PRINCETON, NEW JERSEY USA

G. Reichert

TECHNISCHE UNIVERSITÄT BRAUNSCHWEIG
BRAUNSCHWEIG, GERMANY

August 30-September 1, 1995
SAINT-PETERSBURG, RUSSIA

Paper nr.: VII.8

The Effect of Inflow Models on the Dynamic Response of Helicopters.

U.T.P. Arnold; J.D. Keller; H.C. Curtiss; G. Reichert

TWENTY FIRST EUROPEAN ROTORCRAFT FORUM
August 30 - September 1, 1995 Saint-Petersburg, Russia

THE EFFECT OF INFLOW MODELS ON THE DYNAMIC RESPONSE OF HELICOPTERS

Uwe T.P. Arnold, Jeffrey D. Keller, H.C. Curtiss
Princeton University
Princeton, New Jersey USA

Günther Reichert
Technische Universität Braunschweig
Braunschweig, Germany

Abstract

This paper examines in detail some modifications to the main rotor aerodynamic modeling that will effect the off-axis response of a helicopter. Three different approaches are examined: an extended version of momentum theory including wake distortion terms, a first-order aerodynamic lag model, and an aerodynamic phase correction. It is shown that all three approaches result in similar off-axis responses when applied to a simplified model of the coupled pitch-roll dynamics in hover. Numerical values for the inflow parameters are determined using system identification and are compared to theoretical predictions and previously identified values. Comparisons are also made between a nonlinear simulation model with extended momentum theory and flight test data for a UH-60 in hover, demonstrating considerable improvement in the off-axis response prediction.

Notation

a	Blade lift curve slope
a_1, b_1	Multi-blade flapping coordinates
A_1, B_1	Lateral and longitudinal cyclic pitch
C_T, C_L, C_M	Rotor aerodynamic thrust, roll, and pitch moment coefficients
$G_{A1\text{-}lat}$, $G_{B1\text{-}long}$	Cyclic pitch-to-stick gearings
K_L	Dynamic inflow static gain coefficient, $K_L = a\sigma/16v_o$
K_R, K_T	Wake distortion parameters due to rate and translation
$\hat{L}_{aero}$, $\hat{M}_{aero}$, $\tilde{L}_{aero}$, $\tilde{M}_{aero}$	Reduced aerodynamic moments, defined as $C_{L,M}/K_L v_o$
L_{b_1}, M_{a_1}	Body roll and pitch moment due to tip path plane tilt, e.g. $L_{b_1} = \frac{\partial L/\partial b_1}{I_x\Omega^2}$
M_F	Reduced aerodynamic flap moment in rotating frame
p, q	Body angular rates, nondim. by Ω
R	Rotor radius
v_c, v_s	Harmonic induced velocity components, nondim. by ΩR
v_o	Steady-state uniform induced velocity component, $v_o = \sqrt{C_T/2}$
β	Flap angle in rotating frame
γ	Lock number
γ^*	Reduced Lock number, $\gamma^* = \gamma/(1+K_L)$
δ_{lat}, δ_{long}	Lateral and longitudinal stick position
μ_x, μ_y	Longitudinal and lateral advance ratios at rotor hub
ν	Flapping frequency ratio
σ	Rotor solidity
τ_i	Inflow time constant, nondim. by Ω^{-1}
τ_L	Aerodynamic lag time constant, nondim. by Ω^{-1}
φ	Effective swashplate phase angle (including steady lag angle)
ψ	Azimuth angle
ψ_a	Aerodynamic phase angle
Ω	Rotor rotational speed
$(\,)'$	$d(\,)/d\psi$
$(\,)_{ss}$	Steady-state value

Presented at the Twenty-first European Rotorcraft Forum, St. Petersburg, Russia, August 1995.

Introduction

The reliable prediction of the dynamic response of helicopters to arbitrary control inputs is a fundamental goal in the areas of simulation, handling qualities assessment, and flight control system design. Although

intensive efforts have been undertaken to improve the broad variety of existing dynamic models, their capability of predicting certain aspects of the helicopter response is still poor. One important example is the coupled or off-axis response to cyclic control inputs. Many studies have shown that the agreement with flight test is quantitatively and qualitatively poor, i.e. not only the amplitude but also the sign of the off-axis response is calculated erroneously [1-3]. One common way of circumventing this problem is to use system identification methods based on linear models to obtain numerical coefficients in the equations of motion which will satisfactorily predict the response of a specific rotorcraft [4,5]. Unfortunately, this approach does not tend to illuminate the physical source of the modeling error, and thus the range of application of the identified equations is not clear.

It seems likely that a missing element of the model is associated with some aspect of the aerodynamics. While some of the answers might be found by using a dynamic free wake model, such models are not currently available and in any case would be difficult to couple to a flight dynamics model. Recently, an interesting new approach to some aspects of rotor aerodynamics has been studied by Rosen and Isser [6]. By considering the relative motion between the tip vortices and blades, they have shown significant effects on the off-axis flapping of a rotor due to angular rates. Their approach, however, is computationally intensive and difficult to incorporate directly in a flight dynamics program.

This paper examines three simple models that show possible sources of the off-axis discrepancies. The first model, referred to as extended momentum theory, is developed in [7]. This theory is derived to include the effect of angular velocity, which is omitted from existing dynamic inflow models based on momentum theory. The other two models are based on the concept of a lift deficiency function. This approach was used in the identification study of [8]. The values used in the paper, however, are difficult to justify from classical, two-dimensional unsteady airfoil theory.

The objectives of this paper are to explore the differences in these models, especially as related to the off-axis response, and to see whether system identification methods might distinguish between these models. Following a brief description of the model, analytical and numerical comparisons are made between the three approaches. System identification is used to extract the parameters of the inflow model from flight test data. Comparisons are also made between a nonlinear simulation model and test data using adjusted inflow parameter values.

Coupled Pitch-Roll Dynamics Model

To provide insight into the effects of cross-coupling and their impact on the dynamic response, a low order model of the pitch and roll dynamics is used. This model is extended from the third-order, body-flap approximation used by Curtiss [9] to include the progressing flap mode. The primary terms considered include pitch and roll rates as well as the motion of the tip path plane (a_1, b_1). The basic structure of the model is shown schematically in Fig. 1. Since the translational motion and the lag dynamics do not strongly couple in the frequency range of interest, they are neglected in the model.

The coupling of the pitch and roll motions primarily result from inertial and aerodynamic sources. The largest cross-coupling terms arise from the gyroscopic moments due to flapping and shaft rates and from the aerodynamic model (shown as a dashed box in Fig. 1). Weak sources of coupling also exist due to non-zero hinge offset and body angular accelerations. Because the inertial terms are known and are not directly affected by the inflow model, the remainder of this paper will focus on the aerodynamic model.

To demonstrate the validity of the approximate model, a comparison is made to the nonlinear model, ARNHEL, which includes all fuselage degrees of freedom as well as flap and inflow dynamics [10]. The numerical values used for most calculations are listed in Table 1 and have been chosen to represent the UH-60 helicopter. Figures 2 and 3 show on-axis and off-axis frequency response diagrams for both models with a comparison to flight test data for a hovering UH-60 helicopter, taken from the RASCAL flight test program. From both figures, it is apparent that the approximate model captures the important features of the nonlinear simulation. However, since both models use conventional aerodynamic models, the off-axis response prediction contains a 180 degree phase error. This error is consistent with the errors observed in other investigations.

Rotor Aerodynamic/Inflow Models

In this section, three possible models for calculating the main rotor aerodynamic loads and their effect on the dynamic response are discussed and compared.

Extended Momentum Theory

Finite state inflow models (dynamic inflow) are in widespread use throughout the rotorcraft community. How-

ever, these theories do not include any direct effect of shaft and tip path plane rates. A new induced velocity model, which includes the dominant effects of shaft rate, is presented in [7] and is extended here to include the effects of tip path plane rates. Physically, it seems inconsistent to include the effect of body rates without including tip path plane rates. The non-dimensional equations governing the dynamics of the harmonic induced velocity components are:

$$\begin{aligned} \tau_i v_c' + v_c &= -K_L \hat{M}_{aero} + K_T \mu_x + K_R\left(q + a_1'\right) \\ \tau_i v_s' + v_s &= -K_L \hat{L}_{aero} - K_T \mu_y + K_R\left(p + b_1'\right) \end{aligned} \quad (1)$$

This model is equivalent to the Pitt-Peters dynamic inflow model of [11] when the last term is discarded.

The second and third terms on the right hand side of Eq. (1) are referred to as wake distortion effects due to translation and rate, respectively. The term K_T arises from the "blow back" of the wake due to translation and is thus called a wake distortion effect. The term K_R is a new effect, developed in [7] by Keller, and arises from the curvature of the wake due to pitch rate (see Fig. 4). The simplified, vortex-tube analysis of [7] results in a theoretical value of K_R equal to 1.5, as opposed to the analysis of Rosen and Isser in [6] which apparently yields an equivalent value of K_R less than 1.

Parameter	Value	Units
R	8.18	m
Ω	27	rad/sec
L_{b_1}	0.057	
M_{a_1}	0.0087	
v_o	0.050	
τ_i	2.2	
K_L	0.59	
γ	8.3	
γ^*	5.2	
ν	1.035	
$G_{A1\text{-}6c}$	0.028	rad/in
$G_{B1\text{-}long}$	-0.049	rad/in
φ	7	deg

Table 1. Helicopter parameter values used in numerical calculations.

The induced velocity couples with the body/flap dynamics by changing the aerodynamic moments on the rotor, which in turn feedback to the induced velocity. The effect of wake distortion can be treated as an additional source of aerodynamic coupling. Representing the effects of Eq. (1) on the aerodynamic moments results in the signal flow diagram shown in Fig. 5a. If it is assumed that the induced velocity changes instantaneously ($\tau_i = 0$), the aerodynamic moments reduce to algebraic expressions, simplifying the diagram (see Fig. 5b). From this, it is apparent that aerodynamic coupling results only from tip path plane and shaft rates and that the coupling is suppressed when K_R equals 1.

The primary effect of the wake distortion due to rate is in the off-axis response, as shown in Fig. 6. As K_R is increased to 1, the off-axis amplitude decreases at low frequencies, a direct result of the reduced aerodynamic coupling. As K_R is further increased, the coupling reverses, resulting in an amplitude increase and phase shift of 180 degrees. To match flight test data (shown in Figs. 2 and 3), the wake distortion parameter clearly must take on a value greater than 1.

Another feature of the response is the appearance of an amplitude peak at approximately twice the rotor speed, indicating a reduction in damping of the progressing flap mode. This loss in damping is directly related to the assumed dependence of induced velocity on tip path rate and is related to the inflow time constant as well as K_R. This is illustrated in Fig. 7, which shows a plot of the τ_i-K_R stability boundary for the progressing flap mode. For values above 1, the inflow time constant is approximately equal to the wake distortion parameter on the stability boundary.

Aerodynamic Lag

As shown in the previous section, the rate distortion terms in the inflow affect the aerodynamic cross-coupling leading to modified rotor moments. Similar effects are obtained assuming that the aerodynamic load on each rotor blade lags the change in angle of attack. This is conceptually equivalent to the application of the Theodorsen lift deficiency function [12]. In the present analysis, the equation representing the dynamics of the aerodynamic flap moment in the rotating frame is approximated as a first order system:

$$\tau_L M_F' + M_F = -\left(\tilde{M}_{aero}' \cos\psi + \tilde{L}_{aero} \sin\psi\right) \quad (2a)$$

where

$$\tilde{M}_{aero} = A_1 - a_1' - b_1 - q$$
$$\tilde{L}_{aero} = B_1 - b_1' + a_1 - p \qquad (2b)$$

The term M_F is the normalized aerodynamic moment in the flapping equation for a single blade:

$$\beta'' + \nu^2\beta = \tfrac{\gamma}{8} M_F \qquad (3)$$

Note that the time constant τ_L in Eq. (2a) is also a non-dimensional quantity. In general, Eq. (2b) also depends on the harmonic induced velocity components, v_c and v_s. These effects can be represented by defining an equivalent reduced Lock number, as shown in [13].

Transforming Eq. (2a) to the non-rotating frame results in the following coupled system:

$$\tau_L\left(\hat{M}'_{aero} + \hat{L}_{aero}\right) + \hat{M}_{aero} = \tilde{M}_{aero}$$
$$\tau_L\left(\hat{L}'_{aero} - \hat{M}_{aero}\right) + \hat{L}_{aero} = \tilde{L}_{aero} \qquad (4)$$

In Eq. (4), the terms $\hat{M}_{aero}$ and $\hat{L}_{aero}$ represent the moments in the multi-blade flapping equations:

$$a_1'' + \ldots = \tfrac{\gamma}{8}\hat{M}_{aero}$$
$$b_1'' + \ldots = \tfrac{\gamma}{8}\hat{L}_{aero} \qquad (5)$$

The corresponding signal flow representation is shown in Fig. 8a. It is clear from the diagram that this dynamic "filter" introduces additional cross-coupling between the aerodynamic rotor moments.

The effect of the aerodynamic lag on the on-axis and off-axis frequency responses is illustrated in Fig. 9. Again, increasing τ_L only has significant effect on the off-axis response. In this example, minimum coupling is observed for τ_L equal to 0.33, while double this value yields almost unchanged amplitude but a 180 degree phase shift when compared to the τ_L = 0 case. In general, these results are quite similar to the wake distortion case, except the destabilizing effect of τ_L on the progressing flap mode is much smaller.

It should be noted that the values used in these calculations are much larger than theoretical estimates. For example, the two-dimensional analysis of Theodorsen results in an equivalent value of τ_L of approximately 0.1 at the blade tip for the UH-60.

Aerodynamic Phase Correction

It is suggested in [8] that the off-axis discrepancies can be accounted for by a phase shift in the aerodynamic flapping moment. If the dynamic terms on the left side of Eq. (4) are neglected, the cross-coupling associated with the time constant τ_L persists. The resulting aerodynamic block in the signal flow diagram is shown in Fig. 8b. By defining an equivalent aerodynamic phase angle:

$$\psi_a = \tan^{-1}\left(\tau_L\right) \qquad (6)$$

this corresponds to a simple azimuthal rotation of the aerodynamic moments relative to the angle of attack and a moment reduction by the factor cos ψ_a (see Figs. 8b and 8c). This approach is similar to that of [8], except there the magnitude of the moments is amplified by (1/cos ψ_a).

Figure 10 presents the effect of the phase angle on the response. For these calculations, the aerodynamic moments have been rotated and scaled by the factor cos ψ_a. The results are very similar to both Figs. 6 and 9. The effect of rotating and scaling the aerodynamic moments is illustrated in Fig. 11. When the moments are amplified by (1/cos ψ_a), the on-axis gain is correspondingly increased compared to the ψ_a = 0 reference case. For the on-axis response to be unaffected when including the phase correction, it is necessary to reduce the amplitude of the moments by cos ψ_a, the exact result of the steady-state form of the aerodynamic lag model.

From Figs. 10 and 11, it can be seen that the progressing flap mode is again destabilized, but not nearly as much as with the wake distortion inflow model for an equivalent off-axis response. These results suggest that the only way to distinguish between the effect of the different approaches on the off-axis response is through the damping of the progressing flap mode.

Comparison with Flight Test Data

The previous results indicate that it is possible to find values of K_R, τ_L, and ψ_a to best match the flight test data shown in Figs. 2 and 3. The optimal wake distortion parameter, aerodynamic time lag, and phase angle are computed while holding all others parameters fixed in the model. The resulting frequency responses and corresponding values of K_R, τ_L, and ψ_a are shown in Fig. 12. By increasing the aerodynamic parameters, all three models give similar improvement in the correlation with the measured off-axis frequency response. Since the data is limited to 20 rad/sec, well below the progressing flap

mode, it is impossible to differentiate between the effect of the three models on the response.

It should be emphasized that the parameters values required to improve the off-axis correlation are higher than theory. This is especially true for the aerodynamic lag and phase angle models, whose optimal values are considerably higher than that predicted by two-dimensional, unsteady airfoil theory.

Analytical Comparison of Aerodynamic Models

Because of the similarities in the off-axis frequency responses calculated in the previous section, a closer examination into the connection between the different aerodynamic models is necessary. Consider first the non-dimensional equations governing the coupled pitch/roll dynamics:

Body:

$$\begin{aligned} p' &= L_{b_1} b_1 \\ q' &= M_{a_1} a_1 \end{aligned} \qquad (7a)$$

Flap:

$$\begin{aligned} a_1'' + q' + 2\left(b_1' + p\right) &= \tfrac{\gamma^*}{8}\hat{M}_{aero} \\ b_1'' + p' - 2\left(a_1' + q\right) &= \tfrac{\gamma^*}{8}\hat{L}_{aero} \end{aligned} \qquad (7b)$$

The effects of hinge offset are neglected to simplify the following analysis. Furthermore, by neglecting the inflow dynamics, harmonic induced velocity variations are represented by using the reduced Lock number γ^* in Eq. (7b).

A prominent feature of the off-axis frequency response is the second-order zero in the range of the coupled body/regressing-flap mode. Including the effects of wake distortion, the roll rate to longitudinal cyclic transfer function has the following form:

$$\frac{p}{B_1} = \frac{\gamma^*}{8} L_{b_1} \frac{\left(s^2 + M_{a_1}\right)\left(s + \frac{\gamma^*}{8}\left(1 - K_R\right)\right)}{\Delta(s)} \qquad (8)$$

where $\Delta(s)$ is the sixth order characteristic equation of the system. The pitch rate to lateral cyclic transfer function is identical to Eq. (8) except that L_{b1} and M_{a1} are switched. As can be seen, the second-order zero is unaffected by the inclusion of wake distortion effects. However, the steady-state roll rate due to longitudinal cyclic depends on K_R in the following manner:

$$\left(\frac{p}{B_1}\right)_{ss} = \frac{\left(\frac{\gamma^*}{8}\right)^2\left(1 - K_R\right)}{4 + \left(\frac{\gamma^*}{8}\right)^2\left(1 - K_R\right)^2} \qquad (9)$$

Equation (9) clearly demonstrates the sign change in the steady-state response for values of K_R greater than 1.

Similarly, using the steady-state form of the aerodynamic lag model, the steady-state roll rate due to longitudinal cyclic is the following:

$$\left(\frac{p}{B_1}\right)_{ss} = \frac{\left(\frac{\gamma^*}{8}\right)^2\left(1 - \frac{16\tau_L}{\gamma^*}\right)}{4 + \left(\frac{\gamma^*}{8}\right)^2\left(1 - \frac{16\tau_L}{\gamma^*}\right)^2} \qquad (10)$$

The similarity between Eqs. (9) and (10) leads to the following relationship between K_R and τ_L:

$$K_R = \frac{16\tau_L}{\gamma^*} \qquad (11)$$

It should be emphasized that while this relationship is only true for centrally hinged rotors, it is a useful approximation for rotors with moderate hinge offset. This is confirmed by comparing the optimal values of K_R and τ_L required to match the off-axis response in Fig. 12.

Identification of Inflow Parameters

While earlier sections of this paper examined the general effect of the aerodynamic models on the off-axis response, the remainder focuses on the values of the wake distortion parameters which are required to match flight test data. Specifically, system identification methods are applied to more sophisticated, linear and nonlinear models of the coupled dynamics.

The system identification on the linear model is carried out using the CIFER software package, developed by the U.S. Army and Sterling Software for helicopter frequency domain identification. Reference [14] contains a more detailed description of the CIFER methodology. This software is implemented in two steps. First, frequency response pairs and coherence functions are generated using advanced, multi-variable spectral analysis techniques. Once the frequency response database has been created, optimal parameter values which minimize the weighted, least-squares error between model and flight test frequency responses are computed using an iterative, non-linear search routine. The search algorithm has been

applied to a number of high-order, highly parameterized systems and has been found to be robust for these large problems.

The identification model is an extension of the simplified linear model discussed earlier in this paper. The basic model is expanded to include all body translational and rotational degrees of freedom as well as three flapping degrees of freedom (coning and tip path plane tilt). The full, three state Pitt-Peters dynamic inflow model is also implemented and modified to include the additional wake distortion terms due to rate shown in Eq. (1). In addition, small inertial and aerodynamic terms are included in the equations to increase model fidelity and minimize biases on the identified parameters. The final model structure contains a total of 17 dynamic states and is accurate in the frequency range up to 10 rad/sec.

Unlike stability derivative models, the current model is expressed entirely in terms of 16 physical parameters, including the main and tail rotor parameters as well as fuselage inertias. This has the advantage that the model structure is not over-parameterized, resulting in less correlation among the individual parameters. Furthermore, once the search algorithm is fully converged, Cramer-Rao lower bounds are computed for each parameter. The Cramer-Rao bound represents an estimate of the minimum standard deviation of the parameter value and is used as an indicator of parameter insensitivity and correlation. Parameters with high Cramer-Rao bounds are eliminated or fixed at their theoretical values.

The flight test data used in the identification procedure is taken from the RASCAL flight test program, which was conducted on a hovering UH-60 at a gross weight of 14,350 pounds. Measurements were made of fuselage angular rates, linear accelerations, and cockpit control positions. Although a total of 24 frequency response pairs were extracted from the measured data, over half were eliminated because of low coherence, leaving eleven frequency response pairs in the identification.

Identification of the nonlinear model is conducted with the ARNHEL model directly. In this case, the simulation parameters are chosen to minimize the weighted, least-squares error between measured and predicted responses in the time domain. The parameters are identified using the RASCAL flight test data as well as step response data taken during the USAAEFA flight test program. The measured data used in the identification process consist of the fuselage angular rates. To simplify the numerical search routine, only the control offsets and inflow wake distortion parameters are identified.

Linear Model Results

Because of high Cramer-Rao bounds and parameter correlation, the final parameter set was reduced from the original to include only the fuselage inertias and main rotor parameters. The identified values of the parameters relevant to this study are shown in Table 2. The values of the tail rotor parameters as well as the inflow apparent mass terms were held fixed during the identification process, although the harmonic apparent mass terms were increased to values greater than theory to maintain stability of the progressing flap mode. Because of the poorer quality data at low frequencies, the wake distortion parameter due to translation was also fixed in the model structure.

Parameter	Identified Value	Theoretical Value	Ref. [8]
γ	6.5	8.3	8.34
ν	1.023	1.035	1.02
K_R	3.0	1.5	2.2†

Table 2. Comparison of identified and theoretical parameter values († - equivalent value).

Also shown in Table 2 are the theoretical parameter values and identified values from [8]. Note that the aerodynamic phase correction (ψ_a) was identified in [8] instead of the wake distortion parameter (K_R). The value shown in Table 2 is derived using Eqs. (6) and (11). The identified Lock number and flapping frequency in the present study are less than the theoretical values, but are not unreasonable. However, the value of K_R required to match the off-axis response is twice as large as the theoretical value derived in [7].

Figure 13 shows on-axis and off-axis frequency response comparisons between the identified linear model and flight test data. Also shown as a reference is the model with no wake distortion terms due to rate. For both the identified and reference models, the correlation with the on-axis response is good, although the low frequency gain of the identified model is underestimated as a direct result of the decreased value of Lock number. The correlation with the off-axis frequency response is improved significantly when compared to the reference case, a direct result of the extended momentum theory model. The high frequency phase error in the off-axis response is caused by de-weighting the test data based on low coherence.

Nonlinear Model Results

As with the identification of the linear model, high values of the wake distortion parameter due to rate are required for improved correlation with flight test in the nonlinear simulation. Figure 14 shows a comparison between the model with adjusted inflow parameters and the measured roll and pitch rates from a lateral doublet input of the UH-60 RASCAL helicopter. Also shown in Fig. 14 is the model prediction with the Pitt-Peters dynamic inflow theory ($K_R = 0$, $K_T = 0.736$) as a reference case. From this plot, significant improvement is observed in both the on-axis and off-axis responses when K_R and K_T are increased to 3.2 and 0.85, respectively.

Additional comparisons are shown in Fig. 15 with lateral step response data taken from the USAAEFA test program. Again, the response of the model using the Pitt-Peters theory is shown as a reference. From Fig. 15, it can be seen that excellent correlation is obtained in both the roll and pitch response to a lateral input when K_R and K_T are adjusted to 2.9 and 0.61, respectively.

The identification results with both linear and nonlinear models demonstrate that improvement in the off-axis response prediction requires an increase in the value of K_R to approximately double the theoretical value of 1.5. This high value seems to indicate that some other aerodynamic phenomena may be missing from the model. The optimal value of K_T is questionable, however, since the influence of small errors in the initial trim condition tends to mask this low frequency inflow effect.

Conclusions

The effect of three simple aerodynamic models on the response of a helicopter is examined. The models considered in the analysis are an extended form of momentum theory, an aerodynamic lag model, and an aerodynamic phase correction. The first of these is a new model of the induced velocity of a rotor which includes the direct effect of body and tip path plane rates.

The effect of these aerodynamic models on the response of a helicopter are compared using an approximate model of the coupled pitch-roll dynamics. The numerical calculations in this paper demonstrate that all three approaches essentially result in similar on-axis and off-axis responses. The only significant difference is observed in the damping of the progressing flap mode.

System identification is used to determine the extended momentum theory parameters from flight test data for a UH-60 helicopter in hover. Values of the identified parameters are close to theory, except the value of the wake distortion parameter due to rate is approximately twice the theoretical value of 1.5. The identified model closely matches both the on-axis and off-axis frequency responses. Optimal values of the aerodynamic time lag and phase angle are also computed and are found to have equivalent values to the wake distortion parameter.

Identification of the inflow parameters is also done using the ARNHEL nonlinear simulation model, with results similar to the linear model identification. Although the identified value is considerably higher than theory, very good correlation with the off-axis response is attained. The surprisingly large values of the aerodynamic parameters obtained in this study suggest that some other aerodynamic mechanism may be present.

Acknowledgments

This research was supported in part by NASA Ames Research Center Grant NAG 2-561 and by DFG (Deutsche Forschungsgemeinschaft).

References

[1] Takahashi, M.D., "A Flight-Dynamic Helicopter Mathematical Model with a Single Flap-Lag-Torsion main Rotor," NASA TM 102267, USAAVSCOM TM 90-A-004, Feb. 1990.

[2] Ballin, M.G. and Dalang-Secretan, M.A., "Validation of the Dynamic Response of a Blade-Element UH-60 Simulation Model in Hovering Flight," American Helicopter Society 46th Annual Forum, Washington D.C., May 1990.

[3] Chaimovich, M., Rosen, A., Rand, O., Mansur, M.H., and Tischler, M.B., "Investigation of the Flight Mechanics Simulation of a Hovering Helicopter," American Helicopter Society 48th Annual Forum, Washington D.C., June 1992.

[4] AGARD FMP WG-18, "Rotorcraft System Identification," AGARD -LS-178, Oct. 1991.

[5] Fletcher, J.W., "Identification of UH-60 Stability Derivative Models in Hover from Flight Test Data,"

Journal of the American Helicopter Society, Vol. 40, (1), Jan. 1995.

[6] Rosen, A. and Isser, A., "A New Model of Rotor Dynamics During Pitch and Roll of a Hovering Helicopter," *Journal of the American Helicopter Society*, Vol. 40, (3), July 1995.

[7] Keller, J.D., "An Investigation of Helicopter Dynamic Coupling Using an Analytical Model," 21st European Rotorcraft Forum, St. Petersburg, Russia, Aug. 1995.

[8] Takahashi, M.D., Fletcher, J.W., and Tischler, M.B., "Development of a Model Following Control Law for Inflight Simulation Using Analytical and Identified Models," American Helicopter Society 51st Annual Forum, Fort Worth, TX, May 1995.

[9] Curtiss, H.C., "Stability and Control Modeling," *Vertica*, Vol. 12, (4), 1988.

[10] Arnold, U.T.P., "ARNHEL Generic Helicopter Simulation Program, Vol. I: Theory Manual, Vol. II: User's Manual," Princeton University, Princeton, NJ, 1995.

[11] Pitt, D.M. and Peters, D.A., "Theoretical Prediction of Dynamic-Inflow Derivatives," *Vertica*, Vol. 5, (1), 1981.

[12] Dowell, E.H. et al., A Modern Course in Aeroelasticity, Kluwer Academic Publishers, Dordrecht, Netherlands, 1995.

[13] Curtiss, H.C. and Shupe, N.K., "A Stability and Control Theory for Hingeless Rotors," American Helicopter Society 27th Annual Forum, Washington D.C., May 1971.

[14] Tischler, M.B. and Cauffman, M.G., "Frequency-Response Method for Rotorcraft System Identification: Flight Applications to BO-105 Coupled Rotor/Fuselage Dynamics," *Journal of the American Helicopter Society*, Vol. 37, (3), July 1992.

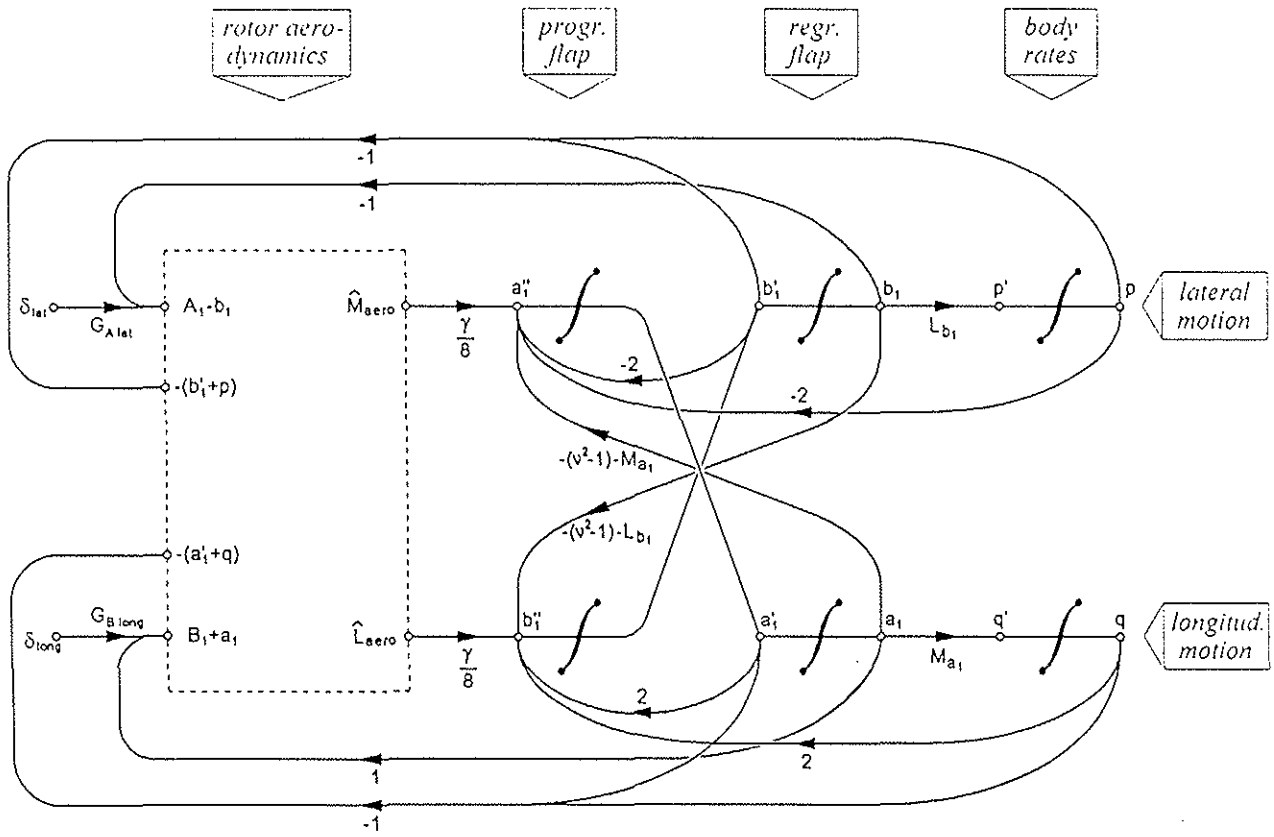

Figure 1 Signal flow diagram of approximate linear model.

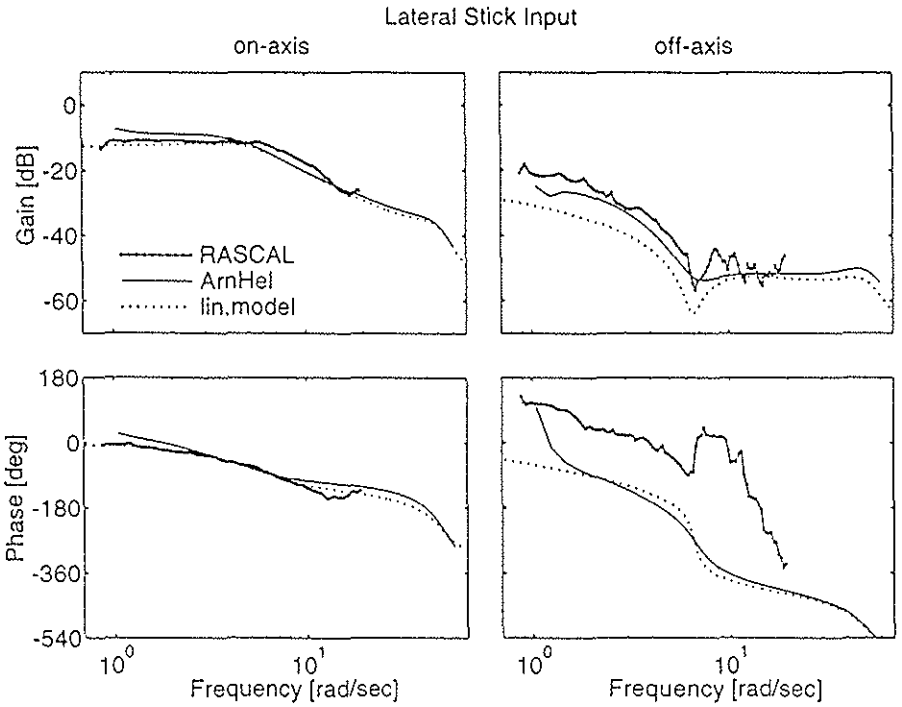

Figure 2 Comparison between approximate model, nonlinear model, and flight test data for UH-60 in hover. (a) On-axis response (p/δ_{lat}), (b) Off-axis response (q/δ_{lat})

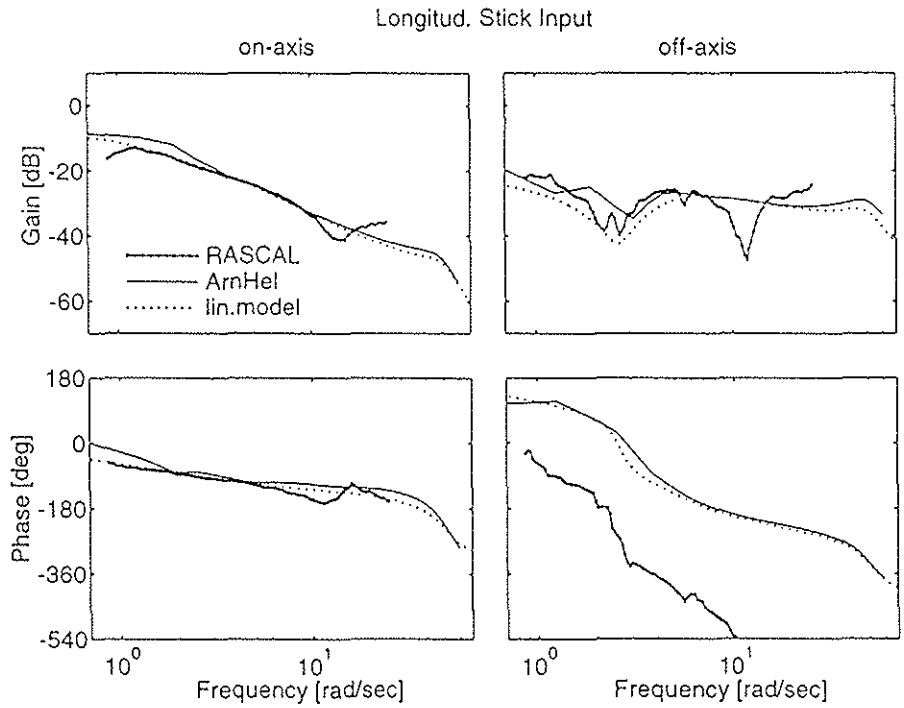

Figure 3 Comparison between approximate model, nonlinear model, and flight test data for UH-60 in hover. (a) On-axis response (q/δ_{long}), (b) Off-axis response (p/δ_{long})

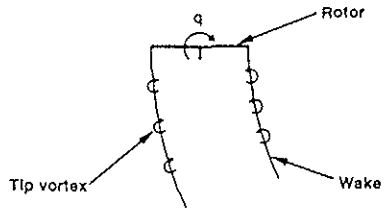

Figure 4 Curved wake structure for rotor undergoing a steady pitch rate.

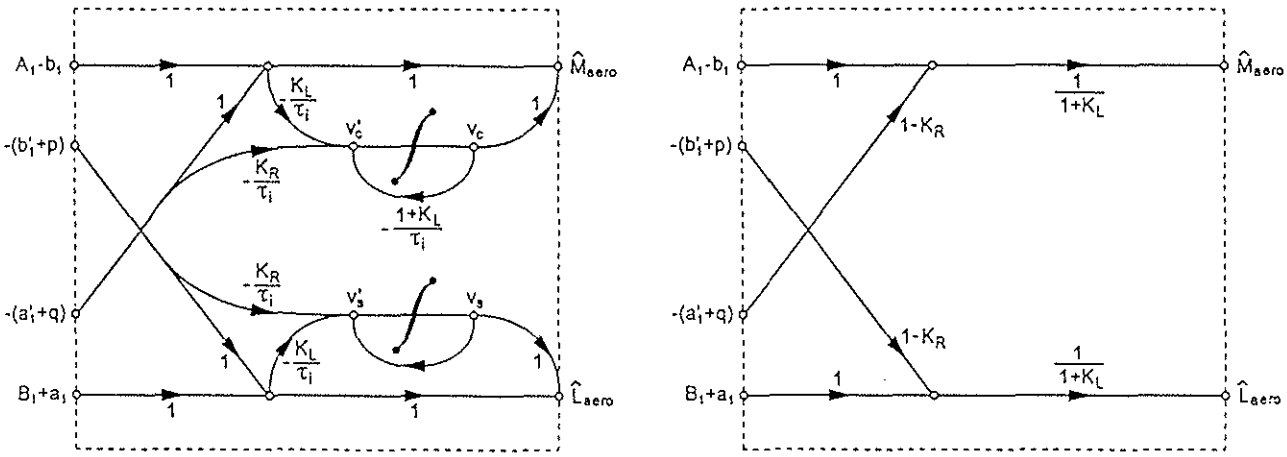

Figure 5 Signal flow diagram of aerodynamic model block using extended momentum theory.
(a) With inflow dynamics (b) Quasi-steady inflow

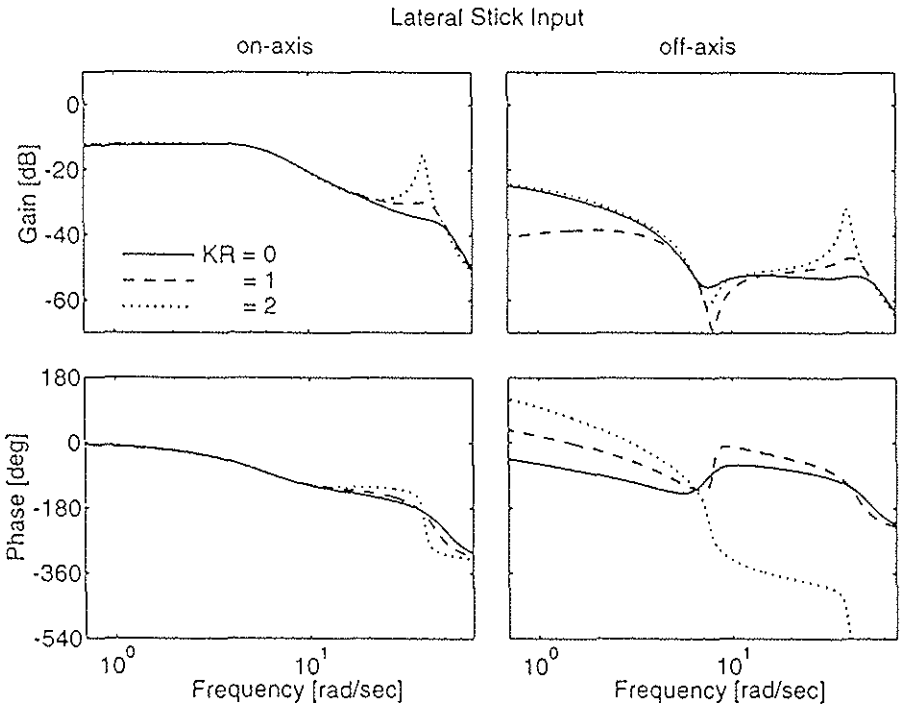

Figure 6 Effect of wake distortion parameter K_R on frequency response.
(a) On-axis response (p/δ_{ls}), (b) Off-axis response (q/δ_{ls})

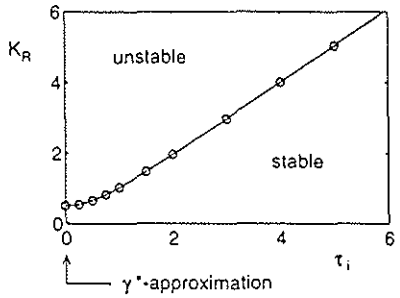

Figure 7 Progressing flap mode stability boundary with extended momentum theory model.

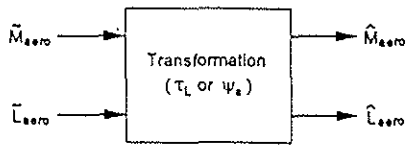

Figure 8 (c) Schematic of flap moment transformation

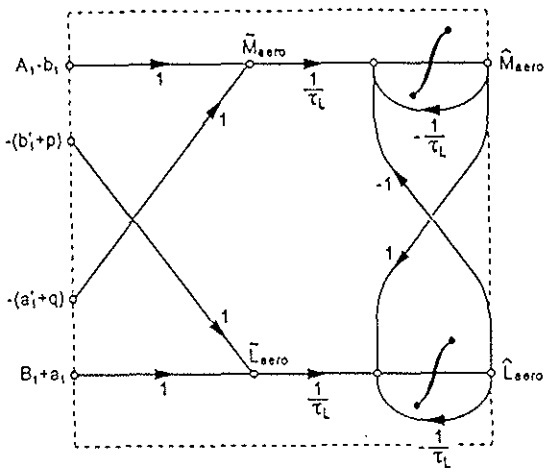

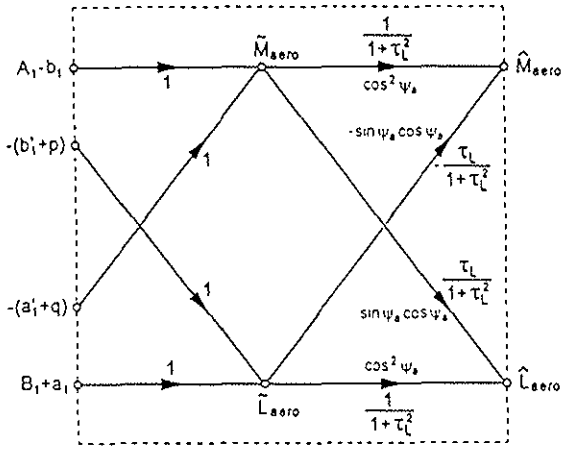

Figure 8 Signal flow diagram of aerodynamic lag model.
(a) Dynamic model (b) Steady-state model

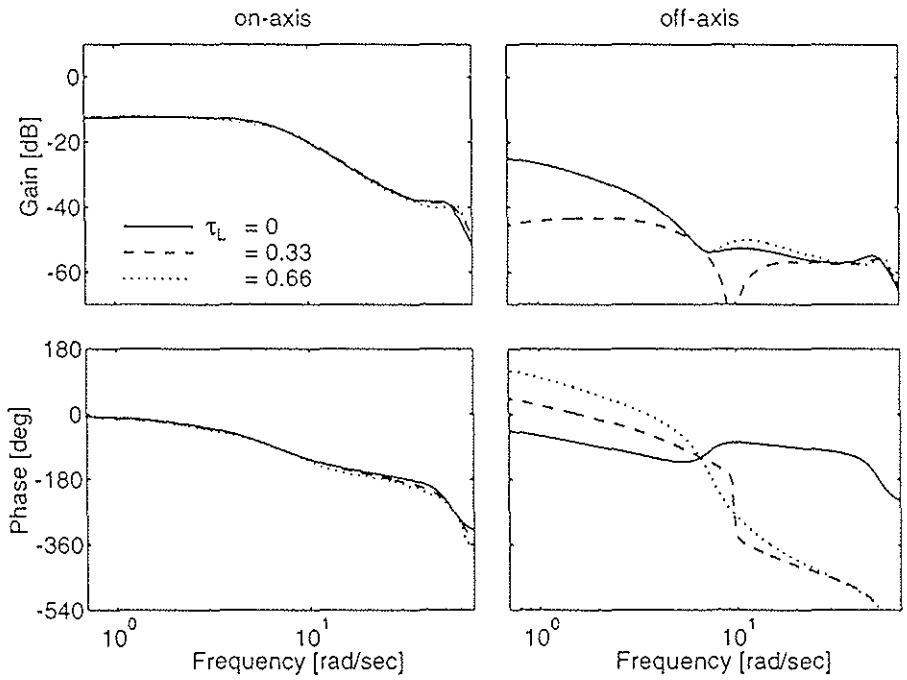

Figure 9 Effect of aerodynamic lag time constant τ_L on frequency response.
(a) On-axis response (p/δ_{lat}), (b) Off-axis response (q/δ_{lat})

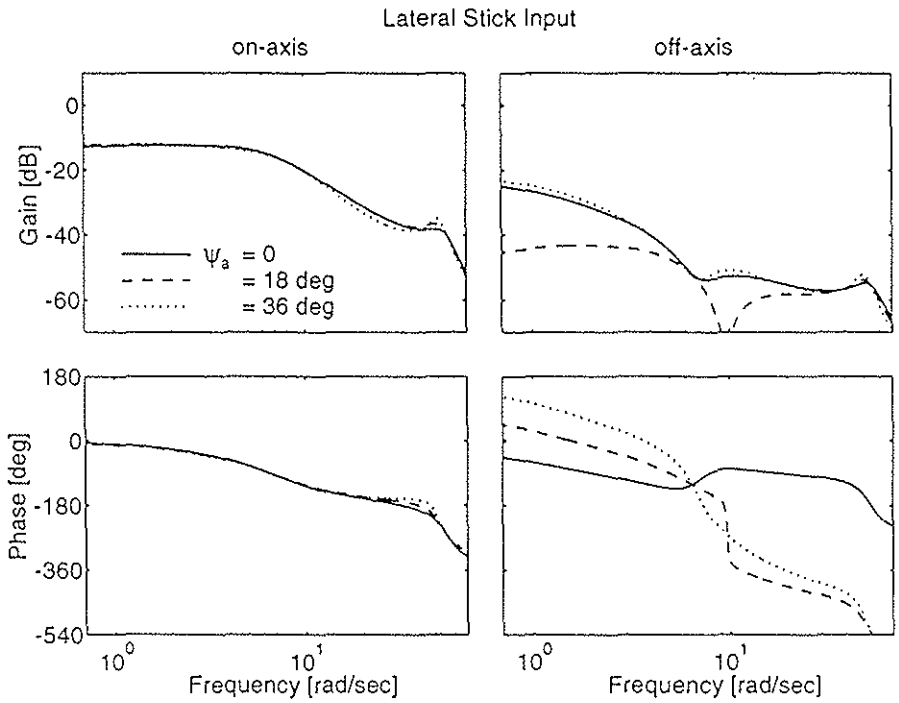

Figure 10 Effect of aerodynamic phase angle ψ_a on frequency response.
(a) On-axis response (p/δ_w), (b) Off-axis response (q/δ_w)

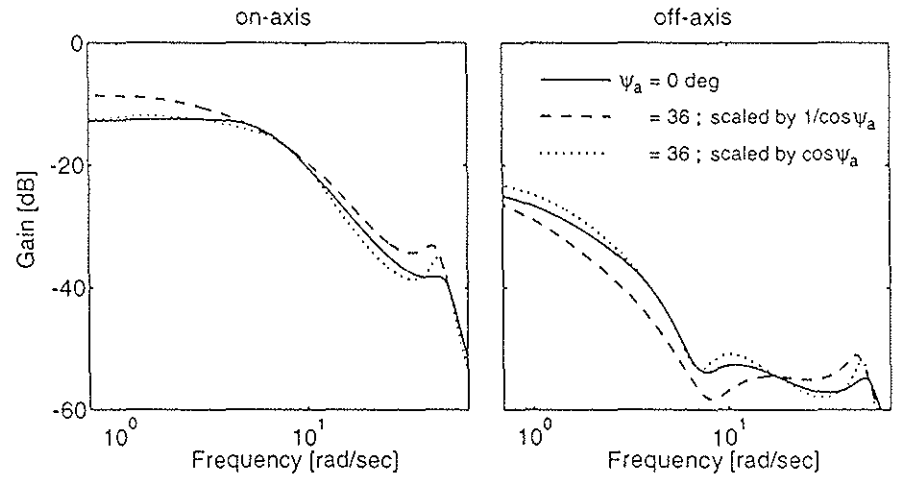

Figure 11 Effect of aerodynamic moment scaling on the response using the aerodynamic phase correction model.

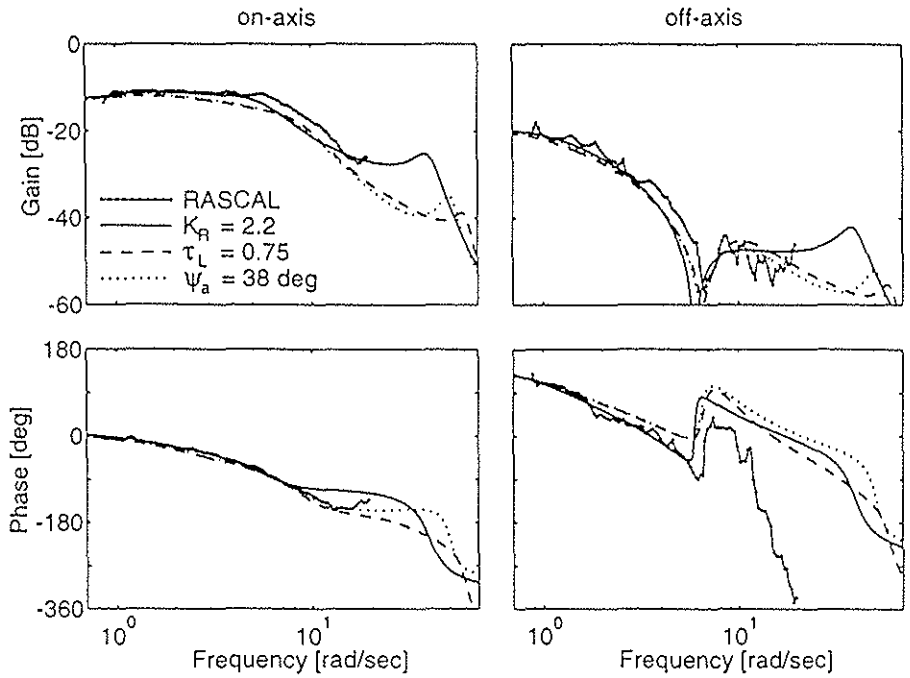

Figure 12 Comparison of approximate linear model frequency response with optimal aerodynamic parameters with flight test data for UH-60 in hover. (a) On-axis response (p/δ_{lat}), (b) Off-axis response (q/δ_{lat})

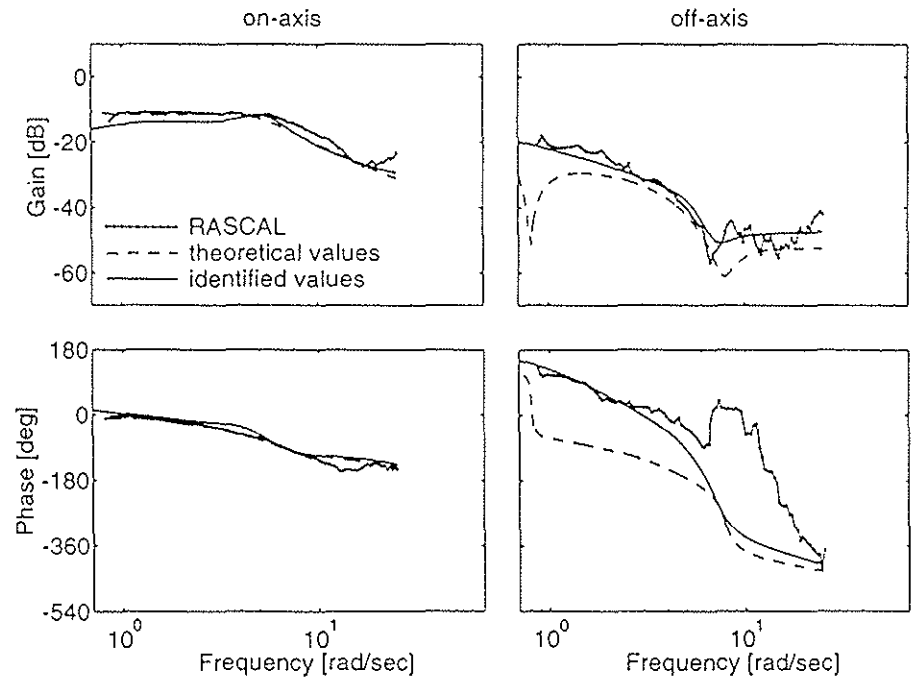

Figure 13 Comparison between identified linear model frequency response and flight test data for UH-60 in hover. (a) On-axis response (p/δ_{lat}), (b) Off-axis response (q/δ_{lat})

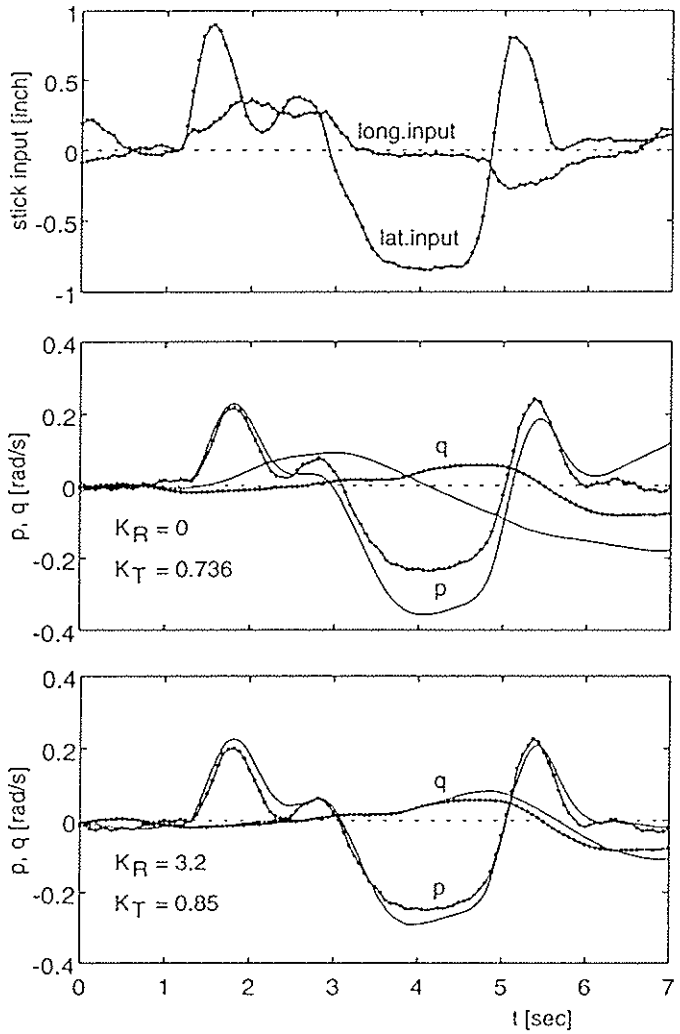

Figure 14 Effect of K_T and K_R on correlation between nonlinear model and lateral doublet response of UH-60 in hover.

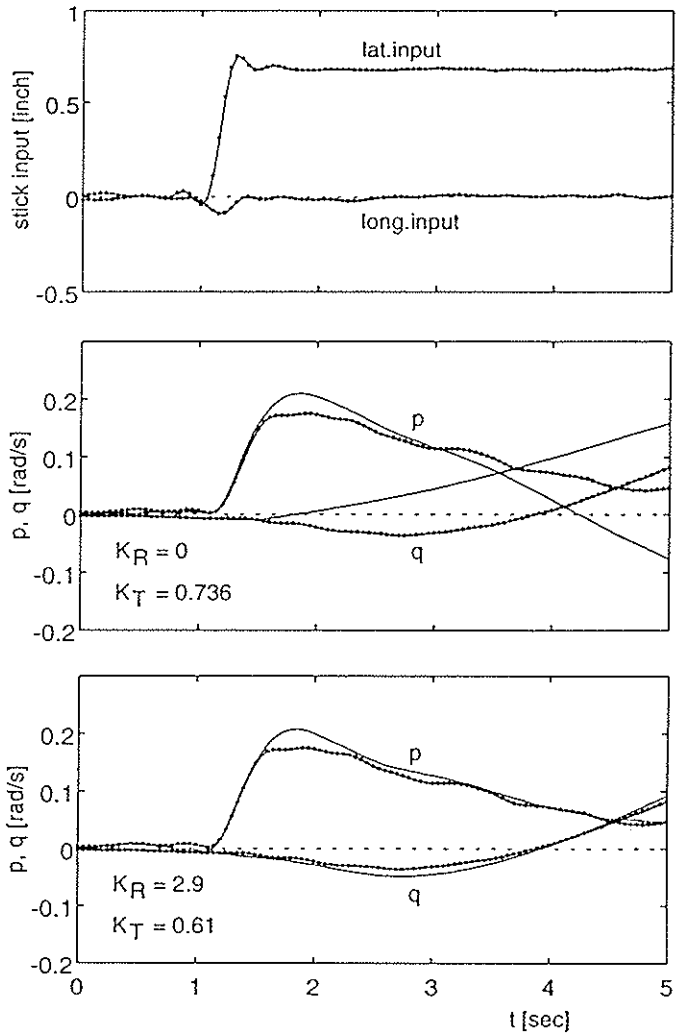

Figure 15 Effect of K_T and K_R on correlation between nonlinear model and lateral step response of UH-60 in hover.